Published in final edited form as:
Gastroenterology. 2013 May ; 144(5): 1055–1065. doi:10.1053/j.gastro.2013.01.053.

Akt and mTORC1 Have Different Roles During Liver Tumorigenesis in Mice

Heidi L. Kenerson[*], **Matthew M. Yeh**[#], **Machiko Kazami**[*], **Xiuyun Jiang**[*], **Kimberly J. Riehle**[*], **Rebecca L. McIntyre**[*], **James O. Park**[*], **Steve Kwon**[*], **Jean S. Campbell**[#], and **Raymond S. Yeung**[*]

[*]Department of Surgery, University of Washington, Seattle, WA

[#]Department of Pathology, University of Washington, Seattle, WA

Abstract

Background & Aims—Phosphatidylinositide 3-kinase (PI3K) is deregulated in many human tumor types, including primary liver malignancies. The kinase Akt and mammalian target of rapamycin complex (mTORC1) are effectors of PI3K that promote cell growth and survival, but their individual roles in tumorigenesis are not well defined.

Methods—In livers of *Alb-Cre* mice, we selectively deleted *tuberous sclerosis* (*Tsc*)*1*, a negative regulator of Ras homolog enriched in brain (Rheb) and mTORC1, along with *Pten*, a negative regulator of PI3K. Tumor tissues were characterized by histologic and biochemical analyses.

Results—The *Tsc1fl/fl;AlbCre*, *Ptenfl/fl;AlbCre*, and *Tsc1fl/fl;Ptenfl/fl;AlbCre* mice developed liver tumors that differed in size, number, and histologic features. Livers of *Tsc1fl/fl;AlbCre* mice did not develop steatosis; tumors arose later than in the other strains of mice and were predominantly hepatocellular carcinomas (HCCs). Livers of the *Ptenfl/fl;AlbCre* mice developed steatosis and most of the tumors that formed were intrahepatic cholangiocarcinomas (ICCs). Livers of *Tsc1fl/fl;Ptenfl/fl;AlbCre* formed large numbers of tumors, of mixed histologies, with the earliest onset of any strain, indicating that loss of Tsc1 and Pten have synergistic effects on tumorigenesis. In these mice, the combination of rapamycin and MK2206 was more effective in reducing liver cell proliferation and inducing cell death than either reagent alone. Tumor differentiation correlated with Akt and mTORC1 activities; the ratio of Akt:mTORC1 activity was high throughout the course of ICC development and low during HCC development. Compared to surrounding non-tumor liver tissue, tumors from all 3 strains had increased activities of Akt, mTORC1, and MAPK and overexpressed fibroblast growth factor receptor (FGFR)1. Inhibition of FGFR1 in Tsc1-null mice suppressed Akt and MAPK activities in tumor cells.

Conclusions—Based on analyses of knockout mice, mTORC1 and Akt have different yet synergistic effects during development of liver tumors in mice.

Correspondence: Raymond S. Yeung, Department of Surgery, University of Washington, 1959 NE Pacific St., Box 356410, Seattle, Washington 98195, USA. Phone: (206) 616-6405 Fax: (206) 616-6406 ryeung@u.washington.edu.

Disclosures: The authors disclose no conflicts.

Author Contributions: Study concept and design (HLK, RSY), data acquisition (HLK, MMY, MK, XY, KR, RLM, JOP, JC), analysis and interpretation (HLK, MMY, JC, RSY), drafting of manuscript (HLK, RSY), critical revision (HLK, MMY, KR, JC, JOP, RSY), statistical analysis (HLK, SK).

Keywords

liver cancer; mouse model; signal transduction; gene disruption

Primary liver cancer, including hepatocellular carcinoma (HCC) and intrahepatic cholangiocarcinoma (ICC) represents the fifth most common malignancy worldwide, with increasing prevalence in the United States [1]. Once diagnosed, most patients are faced with a grim prognosis, and effective systemic therapies remain limited.

One of the 'druggable' pathways known to be disrupted in human HCC is the PI3K/Akt/mTORC1 cascade. Approximately 40% of HCCs showed evidence of Akt activation through epigenetic suppression of *PTEN* by microRNA-21 and mutations or amplification of individual components of the pathway (e.g., PI3KCA, rictor, PTEN, LKB1, TSC1)[2]. While HCCs from all etiologies can be influenced by the PI3K/Akt/mTORC1 pathway, those with underlying nonalcoholic steatohepatitis (NASH) are of particular relevance due to the causal relationship with deregulated insulin signaling. Experimentally, the deletion of *Pten* or over-expression of Akt in mouse livers results in steatosis and tumor development [3,4]. This and other evidence strongly support Akt playing a causative role in hepato-tumorigenesis, but additional mechanisms downstream of Akt remain poorly understood.

Upon growth factor stimulation, mTORC1 phosphorylates S6K1 and 4E-BP1 to promote protein synthesis necessary for cell growth and proliferation[5]. mTORC1 activity is positively regulated by Akt through the phosphorylation and inhibition of two negative regulators, TSC2 and PRAS40. Consequently, when the function of the TSC1/TSC2 complex is lost, mTORC1 becomes constitutively activated, while Akt activity is suppressed through feedback mechanisms mediated by IRS1 and Grb10 [6,7]. Relevantly, a nonsense mutation was detected via whole-genome deep-sequencing analysis in the *TSC1* gene of a human HCV-associated HCC[8]. However, the functional relationship between Akt and mTORC1 in hepatic tumorigenesis is not well defined.

In this study, we examined the effects of constitutive mTORC1 and Akt hyperactivity in mouse models with liver-specific *Tsc1* and/or *Pten* deletion. Comparison of the *Pten*-null model with the *Tsc1*-mutants illustrates differences in lipid metabolism and tumor phenotype. Livers with combined deletion of *Pten* and *Tsc1* showed dramatic synergistic effects on tumor onset and severity and that Akt and mTORC1 influence tumor differentiation. Our results underscore contrasting effects of these two kinases in hepatic tumorigenesis.

Materials & Methods

Mice

$Tsc1^{fl/fl}$ mice were obtained from David Kwiatkowski at Brigham and Women's Hospital (Boston, MA). $Pten^{fl/fl}$ (#006068) and *Alb-Cre* (#003574) mice were purchased from Jackson laboratories (Bar Harbor, ME). $Tsc1^{fl/fl}$ and $Pten^{fl/fl}$ mice were separately bred with *Alb-Cre* mice to generate $Tsc1^{fl/fl}$;Alb^{cre} and $Pten^{fl/fl}$;Alb^{cre} mice respectively. Double knockout (DKO) mutant mice ($Tsc1^{fl/fl}$;$Pten^{fl/fl}$;Alb^{cre}) were created by crossing $Tsc1^{fl/fl}$;Alb^{cre} with $Pten^{fl/fl}$;Alb^{cre} mice to generate $Tsc1^{fl/+}$;$Pten^{fl/+}$;Alb^{cre} mice, and in turn, intercrossed to derive mice with desired genotypes (Supplemental Figure 1). Littermates not carrying the *Cre* alleles were used as controls. Mice were fasted overnight before sacrifice by CO_2 inhalation. All experiments were done in accordance with the Institutional Animal Care and Use Committee (IACUC) at the University of Washington, Seattle.

Cell culture

Human (HepG2) and rat (McA-RH7777) hepatoma cells (ATCC, Manassas, VA) were grown in DMEM with 10% FBS and 1% penicillin/streptomycin. Cells were starved or supplemented with 15% FBS in the presence or absence of inhibitors: rapamycin (50–100nM), AZD8055 (80nM), or MK2206 (500nM) for stated durations. Primary DKO tumor cells were propagated in defined media (DMEM/F12 medium with 15 ng/ml bFGF, 20 ng/ml EGF, 2mM L-glutamine, 4U/l IGF and B27 supplement (1:50)) (Sigma Aldrich). At passage 4, pooled cultures were placed in 10% FBS DMEM/F12 medium and treated with rapamycin (50nM), MK2206 (0.5–1μM) or both for 3 days. Cell proliferation was determined by MTT assay (Sigma Aldrich).

In vivo inhibitor studies

DKO mice were treated with rapamcyin (2 mg/kg, ip) and/or MK2206 (300mg/kg, po), q2days for one week. *Tsc1*−/− mice were treated with PD173074 (20mg/kg, ip, daily for four days). Animals were sacrificed 2 hours following the last dose of drug.

Immunoblot analyses

Mouse liver lysates were analyzed by immunoblot analyses as previously described [9] using antibodies from the following sources: Actin (Sigma, St. Louis, MO), cyclin D1 (Santa Cruz Biotechnology Inc., Santa Cruz, CA), β-catenin (BD Bioscience, San Jose, CA), cytokeratin (CK)-19 (Troma-III) (Developmental Studies Hybridoma Bank, Iowa City, IA), PCNA (DAKO, Carpinteria, CA), HepPar1 (Imgenex, San Diego, CA and DAKO), Sox9 (Millipore, Billerica, MA), Cre and FGFR1 (Novus Biologicals, Littleton, CO). All other antibodies were purchased from Cell Signaling Technology (Danvers, MA).

Mouse RTK array

Mouse Phospho-RTK Array Kits (R&D Systems, Minneapolis, MN) were prepared according to the manufacturer's recommendations. Briefly, 250 μg of protein per sample was placed on individual arrays overnight at 4°C and followed by incubation with diluted Anti-Phospho-Tyrosine-HRP Detection antibody for two hours at room temperature. Signals were detected with chemiluminescent reagents. Densitometry was used to measure relative levels of phosphorylation for each target and non-tumor vs. tumor liver ratios were calculated.

Immunohistochemistry

Tissues were either formalin or methacarn-fixed. Five-micrometer tissue sections were subjected to immunohistochemistry as previously described [9]. TUNEL assay was performed with the In Situ Cell Death Detection Kit (Roche Diagnostics, Indianapolis, IN).

Quantitative RT-PCR

Total RNA was extracted from fresh/frozen liver tissue using TRIzol (Invitrogen, Carlsbad, CA) according to the manufacturer's instructions. qRT-PCR was carried out using pre-designed ABI TaqMan® Gene Expression Assays on an Mx3005P® Multiplex QPCR System (Agilent Technologies) as described [9]. Gene targets included the following: Sox9 (Mm00448840_m1), Krt19 (Mm00492980_m1), Epcam (Mm00493214_m1), and Gpc3 (Mm00516722_m1). Metabolic genes were as previously described [9]. All data were normalized to housekeeping gene, Gapdh averaged over the same time period. Results were expressed as fold-change relative to control liver samples.

Statistical analyses

Quantitative data were analyzed by unpaired t-test and Chi-square test. Categorical data were analyzed by Fischer's exact test. A p-value of less than 0.05 was considered significant. Proportion of mice with gross tumor development was plotted over time for all different genotypes stratified by gender.

Results

Tsc1-null liver tumors do not phenocopy those of the Pten-null model

To study the effects of mTORC1 in hepatic tumorigenesis, we compared the phenotypes of livers with deletion of *Tsc1* or *Pten*. Using the *Cre-loxP* approach, *Tsc1*-floxed and *Pten*-floxed mice were separately crossed with *Alb*-Cre transgenic mice to derive $Tsc1^{fl/fl};Alb^{Cre}$ (a.k.a. *Tsc1*−/−) and $Pten^{fl/fl};Alb^{Cre}$ (a.k.a. *Pten*−/−) mice as described [9]. Liver:body weight ratios were significantly elevated in both models compared to littermate controls (i.e., $Tsc1^{fl/fl}$ and $Pten^{fl/fl}$ without the *Alb-Cre* transgene) although the degree of hepatomegaly was significantly greater in the steatotic *Pten*-null livers compared to the non-steatotic *Tsc1*-null livers (Supplemental Table 1). There was significantly less activity in NAS score in *Tsc1*-null livers (4.3±0.3 (*Pten*−/−) vs. 0±0 (*Tsc1*−/−); p=0.018, Fischer's exact test). Further, serum AST and ALT in the *Tsc1*−/− mice were not elevated compared to $Tsc1^{fl/fl}$ controls (AST: 52.2±4.7 vs. 40.2±5.5, p=0.23; ALT: 28.9±4.6 vs. 52.4±12.4, p=0.10; Student ttest). Despite the lack of steatohepatitis, the *Tsc1*−/− livers were prone to tumor development. At ~1 year of age, the incidence of macroscopic lesions was 50% (9/18) in male and 35% (8/23) in female *Tsc1*−/− livers, and this increased to 85% (11/13) and 77% (10/13), respectively, by 65 weeks of age, compared to 0% in $Tsc1^{fl/fl}$ livers (Figure 1A). The *Pten*-null mice had a significantly higher incidence of macroscopic tumors (At 1 year, male: 100% (12/12), female: 90% (19/21), p<0.01 for both sexes compared to *Tsc1*−/− mice) (Figure 1A). The size and number of tumors were also greater in the 1-yr old *Pten*−/− livers compared to 65-wk old *Tsc1*−/− livers (Figure 1B), suggesting that the tumorigenic effects of *Pten* deletion were more severe than those of *Tsc1* deletion.

Histologic examination of the livers revealed two tumor types, hepatocellular carcinoma (HCC) and intrahepatic cholangiocarcinoma (ICC) and their incidence was significantly different between the *Tsc1*−/− and *Pten*−/− mice. HCC was found in 100% of *Tsc1*−/− livers examined whereas only 22% of *Pten*−/− livers developed HCC (Table 1). Conversely, ICC was noted in 19% of *Tsc1*−/− mice compared to 90% of *Pten*−/− animals (p <0.01). Both models had multi-focal tumors with random distribution in all liver lobes.

HCC from the two models also displayed different histology. In *Pten*−/− mice, HCCs typically showed ballooning and lipid accumulation resembling steatohepatitis in the adjacent, non-tumor liver (Figure 1C); this 'steatohepatitic' variant has been observed in human HCCs, especially in patients with underlying NASH [10]. In contrast, *Tsc1*−/− HCCs closely resembled the classic form of human HCCs with trabecular and pseudoglandular formation in the absence of lipid accumulation (Figure 1C). The morphologic differences in HCCs between the two models paralleled their metabolic phenotypes. qRT-PCR analyses demonstrated that genes involved in lipogenesis (*Srebp1c*, *Fasn*) were up-regulated in *Pten*−/− but not *Tsc1*−/− livers and tumors while other metabolic genes affected in the livers were not different between the *Pten*−/− and *Tsc1*−/− tumors (Figure 1D).

The ICCs from both models shared histologic features that were reminiscent of human ICCs with infiltrative glands surrounded by marked stromal reaction (Figure 1C). Together, our findings indicate that disruption of the Akt/mTORC1 pathway predisposes livers to HCC and ICC that are highly analogous to human cancers. However, tumor phenotype and

incidence were significantly different between the *Tsc1*-null and *Pten*-null models suggesting unique roles of Akt and mTORC1 in liver tumorigenesis.

mTORC1 and Akt have distinct yet synergistic effects on liver tumorigenesis

To further explore the functional interaction of Akt and mTORC1 in tumor development, we created a 'double knock-out' model with liver-specific loss of both *Tsc1* and *Pten* (i.e., $Tsc1^{fl/fl};Pten^{fl/fl};Alb^{Cre}$, a.k.a. DKO). The resultant mutant mice were viable, with body weights comparable to control ($Tsc1^{fl/fl};Pten^{fl/fl}$) littermates. At an early age, DKO mice developed profound hepatomegaly that was significantly greater than either of the single-mutants (Supplemental Table 1). By 14 weeks of age, 100% of DKO-livers showed macroscopic tumors with a disease burden that was similar to that found in 50–60 week old single mutant mice (Figures 1B).

DKO livers contained a high prevalence of both HCC and ICC (Table 1); 58% of DKO livers had mixed tumors which contained elements of HCC and ICC that were intimately intermixed within the context of a single tumor (Figure 1E) as illustrated by immunohistochemical (IHC) analyses using HepPar1 to denote the HCC and CK19 to highlight the ICC components. By 14 weeks of age, microscopic tumors occupied approximately 50% of the DKO liver volume. The dramatic pace of tumorigenesis in these mice was further verified by a high Ki67 index in DKO livers and tumors compared to 'single-mutants' (Figure 1F). Thus, the combined loss of *Tsc1* and *Pten* significantly accelerated tumor development in onset and severity, underscoring the cooperative contributions of Akt and mTORC1.

To further explore if Akt and mTORC1 were acting synergistically, we examined the effects of inhibiting these two kinases in the DKO model. Primary tumor cells were isolated from a DKO tumor, which exhibited a similar biochemical profile as the parental tumors (Supplemental Figure 2A). Treatment with rapamycin or MK2206, allosteric inhibitors of mTORC1 and Akt respectively, significantly suppressed cell growth, and the effects were additive when the drugs were used in combination (Figure 2A); similar results were noted in HepG2 cells (Supplemental Figure 2B). In addition, we treated DKO mice with rapamycin (2mg/kg) and/or MK2206 (300mg/kg) every 2 days for one week. Livers that received the combined drug treatment showed a greater degree of tumor cell death based on the presence of pyknotic nuclei, activated caspase 3, and positive TUNEL staining compared with those receiving single drug treatments (Figure 2B). These *in vitro* and *in vivo* experiments suggest that the combined inhibition of Akt and mTORC1 enhanced anti-tumoral activity and that Akt and mTORC1 acted synergistically during liver tumorigenesis.

Hyper-activation of Akt and mTORC1 in tumors

To explore the molecular pathways involved in tumor development, we compared signaling events in livers from our mouse models. In accordance with the underlying genetic manipulation, non-tumor *Tsc1*−/− livers showed loss of *Tsc1* expression accompanied by increased mTORC1 activity, as reflected by the elevated expression of phospho-S6K1(Thr389) and phospho-S6(Ser235/236) relative to control (Figure 2C, lanes 4,5). Conversely, Akt activity, represented by Akt(Ser473), Akt(Thr308), and GSK3β (Ser9) phosphorylation, was suppressed in *Tsc1*−/− livers secondary to known feedback mechanisms [6, 7]. *Pten*−/− livers showed the opposite pattern with high baseline Akt activity and a subtle increase in mTORC1 activity (Figure 2C, lanes 1,2). The DKO livers had significantly up-regulated Akt and mTORC1 activities, which confirmed the effects of co-deleting *Tsc1* and *Pten* (Figure 2C, lanes 7,8).

Tumors from all 3 models showed accentuation of Akt and mTORC1 activities compared to their respective non-tumor livers (Figure 2C, lanes 3,6,9). In *Pten*-null tumors, elevated S6K1(Thr389) and S6(Ser235/236) phosphorylation were consistent with enhanced Akt activity. However, increased expression of phospho-Akt(Ser473) and downstream effectors, phospho-GSK3(Ser9), and phosopho-PRAS40(Thr246), in *Tsc1*−/− tumors implies the involvement of additional oncogenic event(s) to overcome feedback inhibition of Akt by mTORC1/S6K1 (Figure 2C, Supplemental Figure 3). In this regard, Pten expression was unchanged in *Tsc1*−/− tumors. DKO tumors showed an additive effect with high Akt and mTORC1 activities (Figure 2C, lane 9).

To determine Akt/mTORC1 activation at the cellular level, we performed IHC to identify the cell-specific expression of active Akt and mTORC1. In our hands, commercially available phosho-S6K antibodies do not perform well in IHC (data not shown), so we used its substrate, phospho-S6, as an indicator of mTORC1 activity, and phospho-Akt(Ser473) was used to indicate Akt activity. Figure 2D illustrates the typical patterns of expression of these two phospho-proteins in liver sections from each of the 3 models. Phospho-Akt expression was primarily localized to the plasma membrane where Akt is activated, whereas phospho-S6 was largely cytosolic. In each case, activation of these proteins was higher in tumors compared to adjacent livers as predicted by our immunoblot results. We confirmed the extensive tumor burden of DKO livers by phospho-S6 and phospho-Akt immunostaining, which highlighted the tumor cells (Figure 2E). Importantly, the majority of early tumors (27/32 lesions examined, ~85%), defined as lesions with <30 phospho-S6- or phospho-Akt-positive cells, were situated close to portal/ductal structures where progenitor cells are known to reside (Figure 2E).

Relationship between progenitor cells and tumor development

It has been suggested that mixed HCC-ICC tumors arise from bi-potential progenitor cells[11]. These cells express progenitor markers, such as Sox9, and have been found in the peri-ductal/portal regions of *Pten*-null livers[3, 11, 12]. Among our models, peri-portal Sox9-expressing cells were most abundant in DKO livers and least abundant in *Tsc1*−/− livers (Figure 3A). The over-expression of progenitor cell markers (Sox9, CK19, EpCam, Gpc3) was confirmed by qRT-PCR analyses (Figure 3B). Importantly, the peri-ductal/portal cells in all 3 mutant models expressed PCNA (Figure 3A), suggesting an active state of proliferation, however PCNA expression was not detected in periportal cells of *Alb-Cre*-negative controls (data not shown).

Expansion of Sox9+ cells in our models may be in response to liver injury as noted by Galicia et al. [3] or the direct result of *Cre*-mediated deletion. Lineage tracing experiments in the Alb-Cre mice using a Rosa-26 reporter mouse showed that the albumin promoter is active during early liver development resulting in β–galactosidase activity in post-natal hepatocytes and some cholangiocytes [13]. To determine the relationship between Sox9+ progenitor cells and tumor development in our models, we performed IHC analyses on DKO livers to define the expression of Pten, Tsc1, Cre recombinase, Sox9, HepPar1, CK19, phospho-Akt and phospho-S6 in serial sections. In our hands, commercial antibodies for Tsc1 and Cre were not dependable for IHC analyses (i.e., there was variable background staining in *Tsc1*-null and *Cre*-negative controls respectively). However, the Pten antibody reliably distinguished between *Pten*+/+ and *Pten*−/− cells (Supplemental Figure 4). Thus, we used the absence of Pten immunostaining to indicate *Alb-Cre*-mediated deletion of *Pten* and *Tsc1* in DKO livers. In the non-tumor portion of DKO livers, hepatocytes were uniformly negative for Pten staining while cholangiocytes displayed variable Pten expression, and non-parenchymal cells were consistently positive for Pten and served as an internal control (Figure 4A). Among cholangioctyes, epithelia of large bile ducts routinely retained Pten expression whereas those in small peripheral bile ducts were frequently Pten-negative

(Figure 4A). Periportal Sox9-expressing cells showed a mix of Pten positivity and negativity (Figure 4B). Interestingly, Sox9+;Pten− cells tended to be larger than the Sox9+;Pten+ cells consistent with the effects of mTORC1 on cell size. Examples of peri-portal Sox9+ cells that co-expressed phospho-Akt or phospho-S6 are shown in Figure 4C. These findings suggest that a subset of progenitor cells is both *Pten−/−* and *Tsc1−/−* due to the effects of Alb-Cre.

In DKO tumors, the distribution of Pten expression paralleled that of the non-tumor livers, where HCCs showed uniform loss of Pten expression, while ICCs were either Pten− or + but not both (Figure 4D). In an analysis of 31 ICCs from DKO livers, 17 stained positive for Pten and 14 were negative. In contrast, the proportion of Pten− ICCs was greater in the *Pten*-null livers (i.e., Pten−: 9/11 ICCs, Pten+: 2/11 ICCs. DKO vs. *Pten*-null: X^2=4.40, p=0.04). Both Pten+ and Pten− early ICCs were in close proximity to terminal portal/ductal areas, where abundant Sox9+ cells reside. There was a significant overlap between Sox9 and HepPar1 or CK19 expression in the progenitor cells indicating their bi-lineage potential (Figure 4E). Collectively, our findings in DKO livers show that all HCCs arise from *Tsc1*/*Pten*-deleted cells since they are all phospho-S6+ and Pten−. On the other hand, ICCs were derived either directly from targeted deletion of *Tsc1*/*Pten* (i.e., Pten−) or indirectly from reactive proliferation of Pten+ cells.

Akt and mTORC1 activities correlate with tumor differentiation

The differences in the incidence of HCC and ICC in the *Tsc1−/−* and *Pten−/−* models led us to hypothesize that tumor differentiation is associated with Akt and mTORC1. In IHC analyses of DKO livers, phospho-S6 expression was consistently greater in HCC than ICC, whereas the converse was true for phospho-Akt (i.e., more in ICC than HCC) (Figure 5A). This reciprocal relationship between tumor differentiation and Akt/mTORC1 activities was highly consistent in the early peri-portal tumors as well, whereas MAPK activity was variable among ICCs (Figure 5B, C). Together, these observations suggest that Akt and mTORC1 activities are closely linked to tumor differentiation along the cholangiocytic and hepatocytic lineages, respectively.

Multiple signaling cascades are activated in liver tumors

Cancers evolve from a multi-step process, and molecular events in addition to the loss of *Pten* or *Tsc1* can be expected during tumor development. We found evidence of ERK and Akt phosphorylation in all *Tsc1*-null tumors examined, suggesting upstream receptor tyrosine kinase (RTK) signaling. Previous microarray analyses of *Pten−/−* tumors have shown an elevation of PDGFA expression but not IGF, HGF or EGF[3]. We failed to detect differences in PDGFA or PDGFRa expression in *Tsc1−/−* tumors compared to non-tumor livers (data not shown), but tumor expression of PDGFRb was significantly increased (Figure 6A). In a mouse phospho-RTK array analysis, we confirmed an increase in phosphorylation of PDGFRb along with other receptors including ErbB2 and ErbB3, while the phosphorylation of FGFR3, FGFR4, InsR, Flt-3, TrkC, VEGFR3 and MuSK were notably reduced in *Tsc1−/−* tumors (data not shown). We further found that FGFR1 expression was up-regulated, while EGFR was down-regulated in tumors from all three models (Figure 6A). To determine the cell types associated with PDGFRb and FGFR1 expression, IHC analyses were performed. PDGFRb expression was confined to non-parenchymal cells found within or adjacent to tumors suggesting a potential role of tumor-niche interaction (Figure 6B). FGFR1 is not normally expressed in mature hepatocytes, but was expressed robustly in tumor cells, to a greater extent in HCC than ICC components (Figure 6B). We also detected increased FGFR1 expression in small peri-portal tumors indicating its participation during early tumorigenesis (Figure 6C).

FGFR1 activates the ERK and PI3 kinase pathways upon binding with FGF ligands [14]. In two independent hepatoma cell lines, HepG2 and McA-RH7777, the level of FGFR1 expression was increased with serum stimulation but was not influenced by treatment with rapamycin or a mTOR kinase inhibitor, AZD8055 [15] (Figure 6D) suggesting that the FGFR1 expression was mTOR kinase independent. However, exposure to FGF2 activated Akt and ERK, which were inhibited in the presence of PD173074, a specific FGFR1 inhibitor (Figure 6E). When PD173074 was given to *Tsc1*−/− mice, it effectively inhibited Akt and MAPK activities in *Tsc1*−/− tumors (Figure 6F). These findings identified the potential role of FGFR1 in activating Akt and MAPK signaling in *Tsc1*−/− tumors.

Discussion

By comparing the phenotypes of liver-specific loss of *Tsc1* and/or *Pten*, we discovered that Akt and mTORC1 have common and distinct effects on tumorigenesis. Livers from all three models developed HCC and/or ICC, but the onset and severity of disease varied greatly, and Akt and mTORC1 acted synergistically to promote tumor development. Further, their activities were closely aligned with tumor histology suggesting that Akt promotes cholangiocytic tumors while mTORC1 steers towards hepatocytic lineage. We further identified FGFR1 signaling as an additional oncogenic event that contributes to Akt and MAPK activities in *Tsc1*−/− tumors. These novel insights provide rationale for targeting Akt and mTORC1 in combination for the treatment of primary liver cancers, and our short-term study using rapamycin and MK2206 provides support for this approach.

The *Tsc1*-null model insinuates that the *TSC1* mutation previously identified in human HCC plays a causative role in tumorigenesis [8]. Menon et al. recently reported that HCCs develop in *Tsc1*−/− livers as a result of chronic inflammation/injury secondary to metabolic dysfunction [16]. Compared to *Pten*−/− livers, we found neither histologic nor biochemical evidence of inflammation in our *Tsc1*−/− model. Instead, we attribute *Tsc1*−/− tumorigenesis to the direct oncogenic effects of mTORC1 and Akt activation. The frequency of *TSC1* or *TSC2* mutation in HCC is unknown, but multiple mechanisms can contribute to mTORC1 activation in human HCCs, including the loss of *PTEN*, *LKB1*, or *NF1*, as well as activating mutations of *PI3K* catalytic subunits [2, 17, 18]. IHC studies showed that 25–50% of HCCs have elevated total and phospho-S6K1 and phospho-S6 expression[19, 20]. Correlation analyses found that mTORC1 activation was associated with a greater risk of HCC recurrence, higher tumor stage and moderate/poorly differentiated tumors [18].

Mixed HCC-ICC tumors in humans are thought to originate from bi-lineage progenitor cells or through trans-differentiation of hepatocytes to cholangiocytes [2122]. Our consistent finding of PCNA-positive, Sox9-expressing peri-portal/ductal cells in the vicinity of early tumors supports the progenitor model. We found Sox9+ cells with or without *Pten* deletion in the peri-portal zone. Correspondingly, two groups of ICCs were identified with or without Pten expression. We speculate that the Pten-negative ICC/HCCs are a direct consequence of Akt and mTORC1 activation of Sox9+;Pten− progenitor cells. On the other hand, Sox9+;Pten+ peri-ductal cells may give rise to Pten+ ICCs. The juxtaposition of Pten+ ICC with Pten− HCC in mixed tumors is inconsistent with the concept of trans-differentiation and would also imply independent origins of the two tumor cell types (e.g., a collision tumor). It is unclear why we did not observe any Pten+ HCCs unless the Sox9+;Pten+ progenitors are limited to cholangiocytic differentiation. Further investigations are necessary to determine the role of Akt and mTORC1 in progenitor cell differentiation.

Clinical trials using mTORC1 inhibitors alone in human HCCs have not yielded the expected outcome. In a phase I/II study of Everolimus, only one out of 28 patients had a partial response [23], but results from phase III trials are still pending. Besides tumor

heterogeneity and activation of Akt and MAPK by mTORC1 inhibitors [6, 24], additional oncogenic events such as FGFR1 overexpression can contribute to the apparent lack of activity. Ectopic expression of FGFR1 promotes DEN-initiated hepatocarcinogenesis [25], and FGF signaling plays a critical role in early liver development and the maintenance of hepatic progenitor cells [26]. While the mechanism responsible for FGFR1 up-regulation is currently unknown, FGFR1 inhibitors such as brivanib have shown anti-tumoral activity in human HCC [27] although in phase III trials, brivanib did not meet its primary objective as first-line (BRISK-FL) or second-line treatment (BRISK-PS, BMS press release). The efficacy of FGFR inhibitors in the subset of HCCs showing FGF pathway activation remains to be investigated.

In summary, our models provide unique insights into the contrasting roles of Akt and mTORC1 as primary 'drivers' in the pathogenesis of hepatic neoplasms and support the combined suppression of Akt and mTORC1 signaling in the treatment of these diseases.

Supplementary Material

Refer to Web version on PubMed Central for supplementary material.

Acknowledgments

The cytokeratin 19 antibody (TROMA-III) was obtained from the Developmental Studies Hybridoma Bank developed under the auspices of the NICHD and maintained by The University of Iowa, Department of Biology, Iowa City, IA 52242.

Grant support: Supported by grants from NIH (CA77882 and CA102662).

Abbreviations

mTORC1	mammalian target of rapamycin complex 1
Tsc1	tuberous sclerosis complex 1
DKO	double knock-out
HCC	hepatocellular carcinoma
ICC	intrahepatic cholangiocarcinoma
NASH	nonalcoholic steatohepatitis
NAS score	NAFLD activity score
Alb	albumin
FGFR1	fibroblast growth factor receptor 1
PDGFRb	platelet-derived growth factor receptor beta
Sox9	sex determining region Y-box 9

References

1. Nordenstedt H, White DL, El-Serag HB. The changing pattern of epidemiology in hepatocellular carcinoma. Dig Liver Dis. Jul; 2010 42(Suppl 3):S206–214. [PubMed: 20547305]
2. Zucman-Rossi J. Molecular classification of hepatocellular carcinoma. Dig Liver Dis. Jul; 2010 42(Suppl 3):S235–241. [PubMed: 20547309]
3. Galicia VA, He L, Dang H, et al. Expansion of hepatic tumor progenitor cells in Pten-null mice requires liver injury and is reversed by loss of AKT2. Gastroenterology. Dec; 2010 139(6):2170–2182. [PubMed: 20837017]

4. Calvisi DF, Wang C, Ho C, et al. Increased lipogenesis, induced by AKT-mTORC1-RPS6 signaling, promotes development of human hepatocellular carcinoma. Gastroenterology. Mar; 2011 140(3):1071–1083. [PubMed: 21147110]
5. Zoncu R, Efeyan A, Sabatini DM. mTOR: from growth signal integration to cancer, diabetes and ageing. Nat Rev Mol Cell Biol. Jan; 2011 12(1):21–35. [PubMed: 21157483]
6. Harrington LS, Findlay GM, Gray A, et al. The TSC1–2 tumor suppressor controls insulin-PI3K signaling via regulation of IRS proteins. J Cell Biol. Jul 19; 2004 166(2):213–223. [PubMed: 15249583]
7. Hsu PP, Kang SA, Rameseder J, et al. The mTOR-regulated phosphoproteome reveals a mechanism of mTORC1-mediated inhibition of growth factor signaling. Science. Jun 10; 2011 332(6035): 1317–1322. [PubMed: 21659604]
8. Totoki Y, Tatsuno K, Yamamoto S, et al. High-resolution characterization of a hepatocellular carcinoma genome. Nat Genet. May; 2011 43(5):464–469. [PubMed: 21499249]
9. Kenerson HL, Yeh MM, Yeung RS. Tuberous sclerosis complex-1 deficiency attenuates diet-induced hepatic lipid accumulation. PLoS One. 2011; 6(3):e18075. [PubMed: 21479224]
10. Salomao M, Remotti H, Vaughan R, Siegel AB, Lefkowitch JH, Moreira RK. The steatohepatitic variant of hepatocellular carcinoma and its association with underlying steatohepatitis. Hum Pathol. May; 2012 43(5):737–746. [PubMed: 22018903]
11. Alison MR. Liver stem cells: implications for hepatocarcinogenesis. Stem Cell Rev. 2005; 1(3): 253–260. [PubMed: 17142862]
12. Furuyama K, Kawaguchi Y, Akiyama H, et al. Continuous cell supply from a Sox9-expressing progenitor zone in adult liver, exocrine pancreas and intestine. Nat Genet. Jan; 2011 43(1):34–41. [PubMed: 21113154]
13. Xu X, Kobayashi S, Qiao W, et al. Induction of intrahepatic cholangiocellular carcinoma by liver-specific disruption of Smad4 and Pten in mice. J Clin Invest. Jul; 2006 116(7):1843–1852. [PubMed: 16767220]
14. Kouhara H, Hadari YR, Spivak-Kroizman T, et al. A lipid-anchored Grb2-binding protein that links FGF-receptor activation to the Ras/MAPK signaling pathway. Cell. May 30; 1997 89(5): 693–702. [PubMed: 9182757]
15. Chresta CM, Davies BR, Hickson I, et al. AZD8055 is a potent, selective, and orally bioavailable ATP-competitive mammalian target of rapamycin kinase inhibitor with in vitro and in vivo antitumor activity. Cancer Res. Jan 1; 2010 70(1):288–298. [PubMed: 20028854]
16. Menon S, Yecies JL, Zhang HH, et al. Chronic activation of mTOR complex 1 is sufficient to cause hepatocellular carcinoma in mice. Sci Signal. Mar 27.2012 5(217):ra24. [PubMed: 22457330]
17. Meng F, Henson R, Wehbe-Janek H, Ghoshal K, Jacob ST, Patel T. MicroRNA-21 regulates expression of the PTEN tumor suppressor gene in human hepatocellular cancer. Gastroenterology. Aug; 2007 133(2):647–658. [PubMed: 17681183]
18. Villanueva A, Chiang DY, Newell P, et al. Pivotal role of mTOR signaling in hepatocellular carcinoma. Gastroenterology. Dec; 2008 135(6):1972–1983. 1983 e1971–1911. [PubMed: 18929564]
19. Sahin F, Kannangai R, Adegbola O, Wang J, Su G, Torbenson M. mTOR and P70 S6 kinase expression in primary liver neoplasms. Clin Cancer Res. Dec 15; 2004 10(24):8421–8425. [PubMed: 15623621]
20. Baba HA, Wohlschlaeger J, Cicinnati VR, et al. Phosphorylation of p70S6 kinase predicts overall survival in patients with clear margin-resected hepatocellular carcinoma. Liver Int. Mar; 2009 29(3):399–405. [PubMed: 18492014]
21. Limaye PB, Bowen WC, Orr AV, Luo J, Tseng GC, Michalopoulos GK. Mechanisms of hepatocyte growth factor-mediated and epidermal growth factor-mediated signaling in transdifferentiation of rat hepatocytes to biliary epithelium. Hepatology. May; 2008 47(5):1702–1713. [PubMed: 18398918]
22. Yeh MM. Pathology of combined hepatocellular-cholangiocarcinoma. J Gastroenterol Hepatol. Sep; 2010 25(9):1485–1492. [PubMed: 20796144]

23. Zhu AX, Abrams TA, Miksad R, et al. Phase 1/2 study of everolimus in advanced hepatocellular carcinoma. Cancer. Nov 15; 2011 117(22):5094–5102. [PubMed: 21538343]

24. Carracedo A, Ma L, Teruya-Feldstein J, et al. Inhibition of mTORC1 leads to MAPK pathway activation through a PI3K-dependent feedback loop in human cancer. J Clin Invest. Sep; 2008 118(9):3065–3074. [PubMed: 18725988]

25. Huang X, Yu C, Jin C, et al. Ectopic activity of fibroblast growth factor receptor 1 in hepatocytes accelerates hepatocarcinogenesis by driving proliferation and vascular endothelial growth factor-induced angiogenesis. Cancer Res. Feb 1; 2006 66(3):1481–1490. [PubMed: 16452204]

26. Sekhon SS, Tan X, Micsenyi A, Bowen WC, Monga SP. Fibroblast growth factor enriches the embryonic liver cultures for hepatic progenitors. Am J Pathol. Jun; 2004 164(6):2229–2240. [PubMed: 15161655]

27. Finn RS, Kang YK, Mulcahy M, et al. Phase II, open-label study of brivanib as second-line therapy in patients with advanced hepatocellular carcinoma. Clin Cancer Res. Apr 1; 2012 18(7):2090–2098. [PubMed: 22238246]

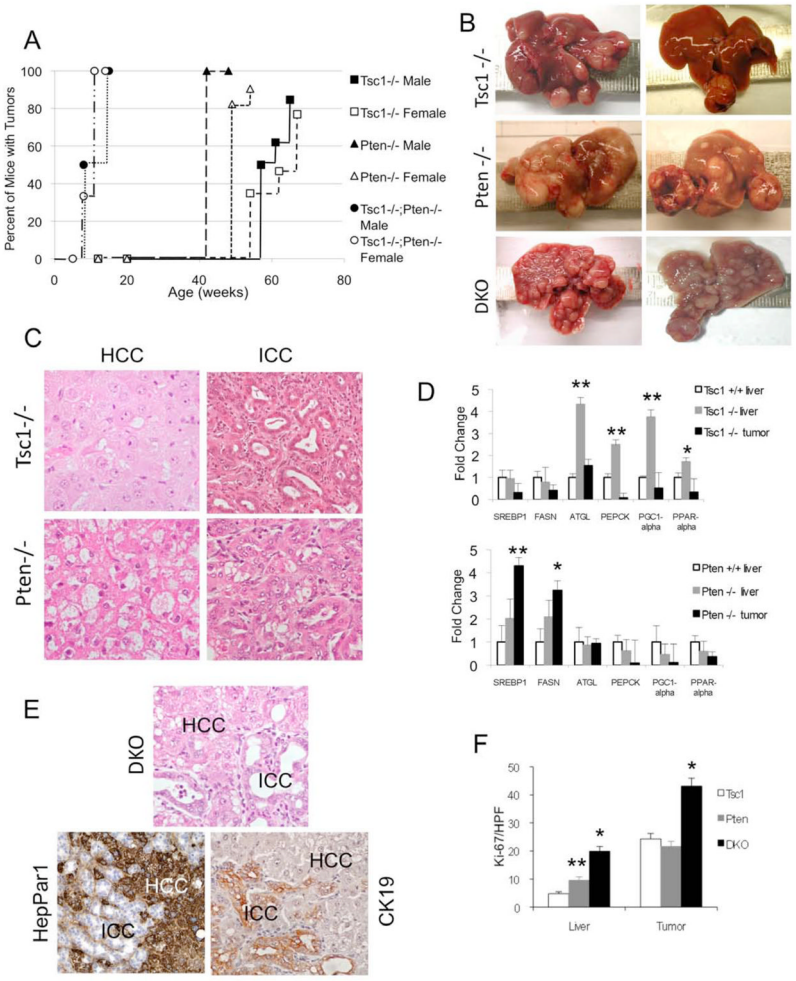

Figure 1.

HCC and ICC in *Tsc1*−/−, *Pten*−/− and DKO livers. A) Incidence of liver tumors in each of the three models: *Tsc1*−/−, *Pten*−/− and *Tsc1*−/−;*Pten*−/− (DKO) mice stratified by sex. Cre-negative control mice did not develop liver tumors over the same time period (data not shown). B) Gross appearances of 64-wk *Tsc1*−/−, 52-wk *Pten*−/−, and 14-wk DKO livers. C) Representative H&E photomicrographs of HCC (left column) and ICC (right column) in *Tsc1*−/− and *Pten*−/− livers. Note ballooning and lipid accumulation in the *Pten*−/− HCC. Magnification: 400X. D) qRT-PCR analyses comparing the expression of metabolic genes in tumor, non-tumor livers and Cre–negative control (*Tsc1*+/+) livers. * $p<0.05$; ** $p<0.01$ compared to control. E) Histologic appearance of a mixed HCC-ICC in a DKO liver. HepPar1 immunoreactivity highlights HCC, and CK-19 highlights ICC. Magnification: 400X. F) Proliferation of non-tumor livers and tumors in each of the 3 models as determined by the number of Ki67-'positive' cells per high power field. Data obtained from 3 mice/group with 5 HPFs each. * $p<0.01$ compared to *Tsc1*−/− and Pten−/−; ** $p<0.05$ compared to *Tsc1*−/−.

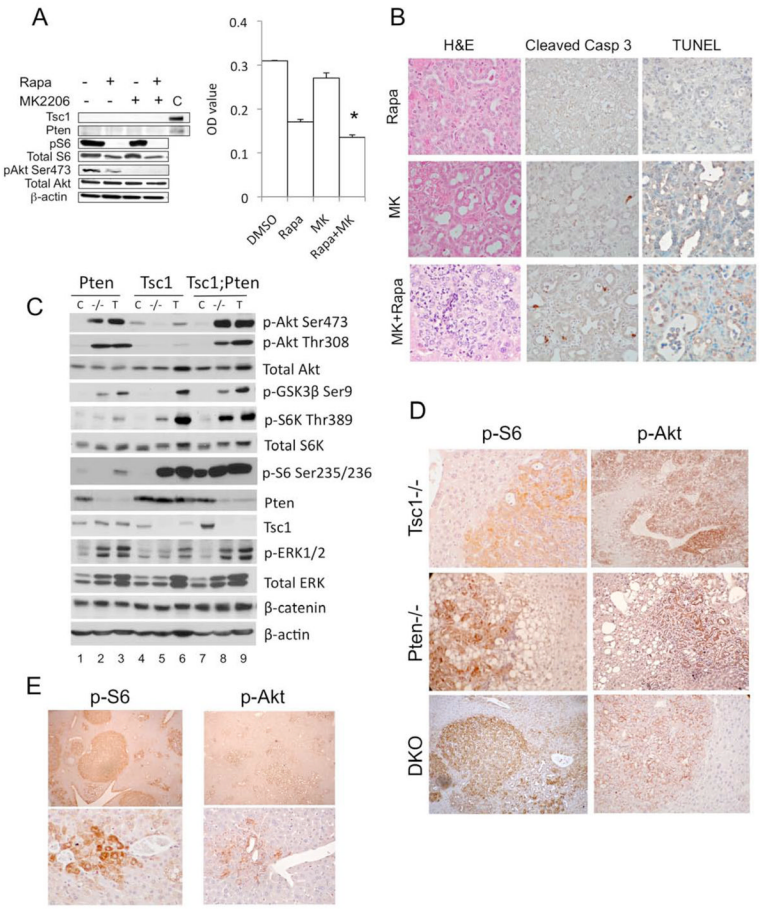

Figure 2.

Synergistic effects of *Tsc1* and *Pten* deletion on tumor development. A) Effects of rapamycin (50nM) and MK2206 (500nM) on the proliferation of primary DKO tumor cells. After a three-day treatment, MTT assay was performed in triplicates and O.D. was measured. Immunoblot shows the intended effects of the inhibitors. C, control. * $p<0.05$ compared to Rapa, $p=0.0001$ compared to DMSO and MK. B) *In vivo* effects of rapamycin (2mg/kg, ip, q2d), MK2206 (300mg/kg, po, q2d) or both after one week of treatment. Representative tumors processed by H&E, cleaved caspase 3 and TUNEL staining. Magnification 400x. C) Immunoblot analyses of livers (−/−) and tumors (T) from the 3 models compared to respective Cre-negative controls (C). D) IHC analyses highlighting phospho-S6 and phospho-Akt expression in tumors of the 3 models. E) Multi-focal tumors in DKO livers highlighted by phospho-S6 and phospho-Akt expression. Bottom: early peri-ductal tumors. Magnification: 40x (top), 400x (bottom).

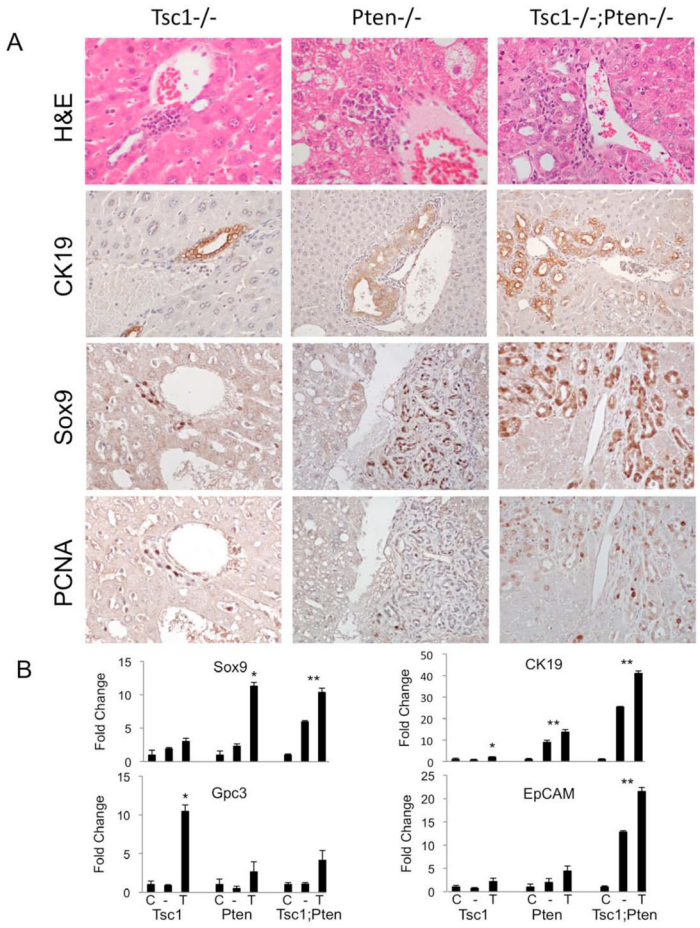

Figure 3.

Loss of *Tsc1* and/or *Pten* is accompanied by an expansion of peri-portal progenitor cells. A) H&E staining shows variable accumulation of peri-ductal/portal cells in the 3 models (Top panels). CK19 expression is largely confined to the biliary epithelial cells. Sox9 and PCNA expression in the periportal regions are shown in serial histologic sections. Original magnification: 400X except for CK19 in *Pten*−/− and *Tsc1*−/−;*Pten*−/− (200X). B) mRNA expression of progenitor markers using qRT-PCR analyses of tissue samples from Cre-negative control livers (C), mutant livers (−), and tumors (T) in each of the 3 models. * $p<0.05$ comparing tumor (T) with non-tumor liver (−) and control liver (C). **$p<0.05$ comparing control liver (C) with non-tumor liver (−) and tumor (T).

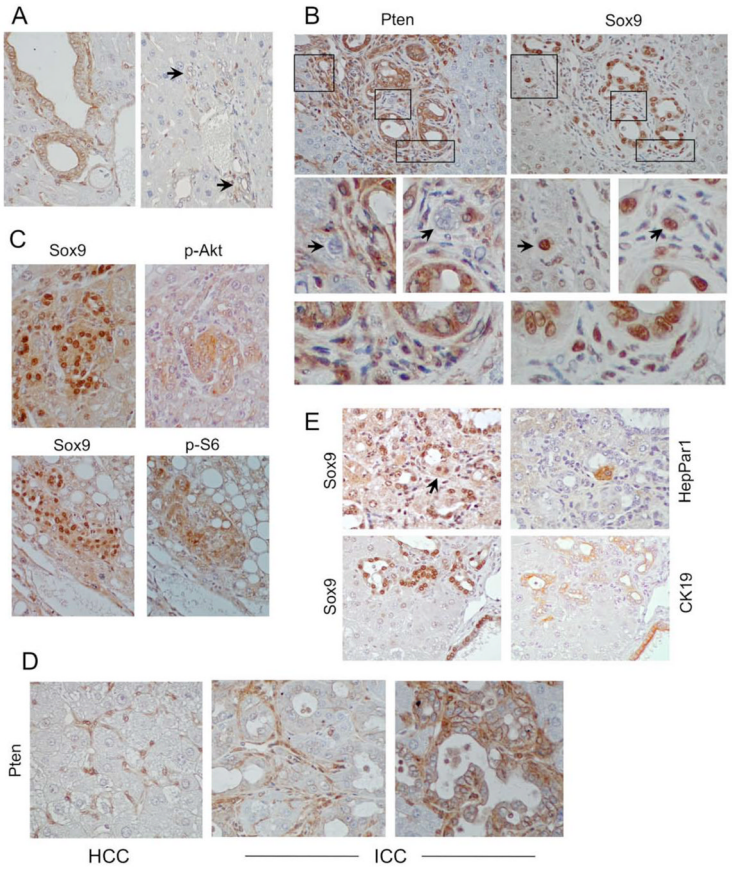

Figure 4.

Sox9-expressing cells in DKO livers. A) IHC analyses of DKO non-tumor livers showing variable Pten expression in cholangiocytes. Arrows indicate small peripheral bile ducts. Note that hepatocytes are uniformly negative while non-parenchymal cells are uniformly positive. B) IHC analyses of peri-ductal cells highlighting Pten and Sox9 expression in serial sections. Boxed areas are magnified below. Arrows point to Sox9'+';Pten'−' cells. Bottom panel highlights immature Sox9'+';Pten'+' cells. Note that matured cholangiocytes were also Sox9'+'. C) Co-expression of Sox9 and phospho-Akt (top) or phospho-S6 (bottom) in peri-portal regions. D) Examples of Pten'−' HCC, Pten'−' ICC, and Pten'+' ICC. Note the presence of Pten'+' stromal cells. E) Examples of Sox9'+';HepPar1'+' (arrow) and Sox9'+';CK19'+' peri-ductal cells. Original magnification: 400X

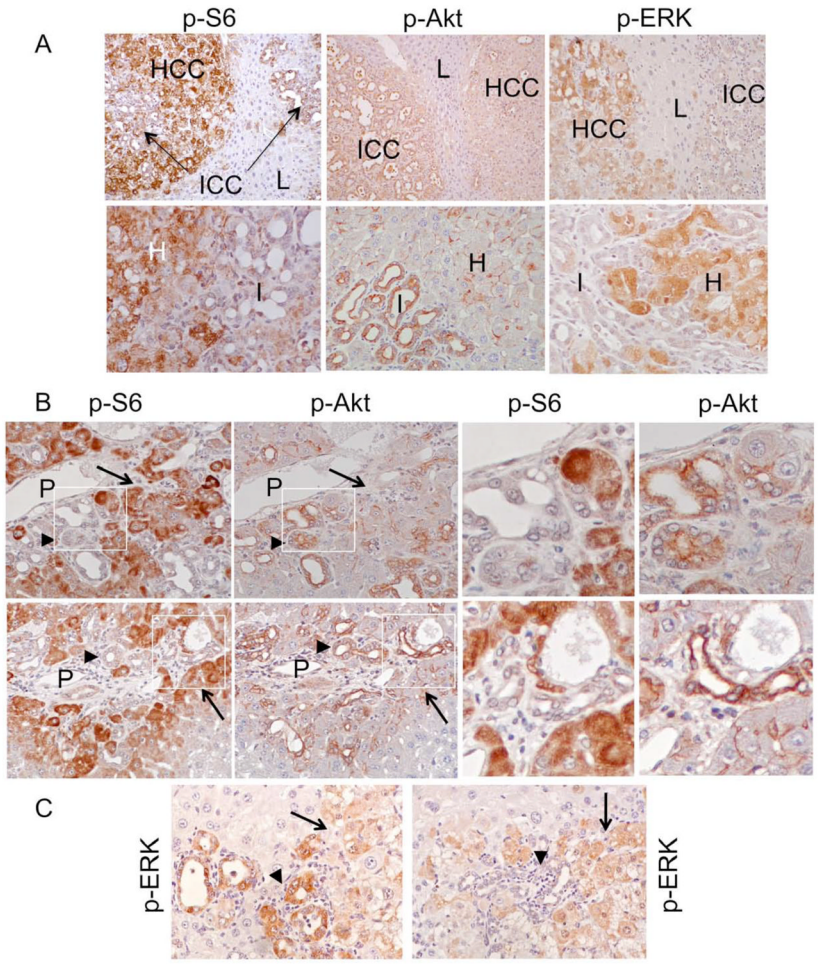

Figure 5.

Relationship between Akt/mTORC1, ERK and tumor differentiation. A) Expression of phospho-S6, phospho-Akt, and phospho-ERK in ICC (I), HCC (H) and adjacent non-tumor livers (L) based on IHC analyses. Top panel: 100x. Bottom panel: 400x. B) Serial sections of two DKO livers showing early peri-portal mixed tumors. Note contrasting phospho-S6 and phospho-Akt expression in the HCC (arrow) and ICC (arrowhead) components. P, portal vein. Left two columns: 400X. Right two columns: high magnification views of the boxed areas. C) Expression of phospho-ERK in two independent early mixed tumors. Arrowhead: ICC. Arrow: HCC. Original magnification: 400X.

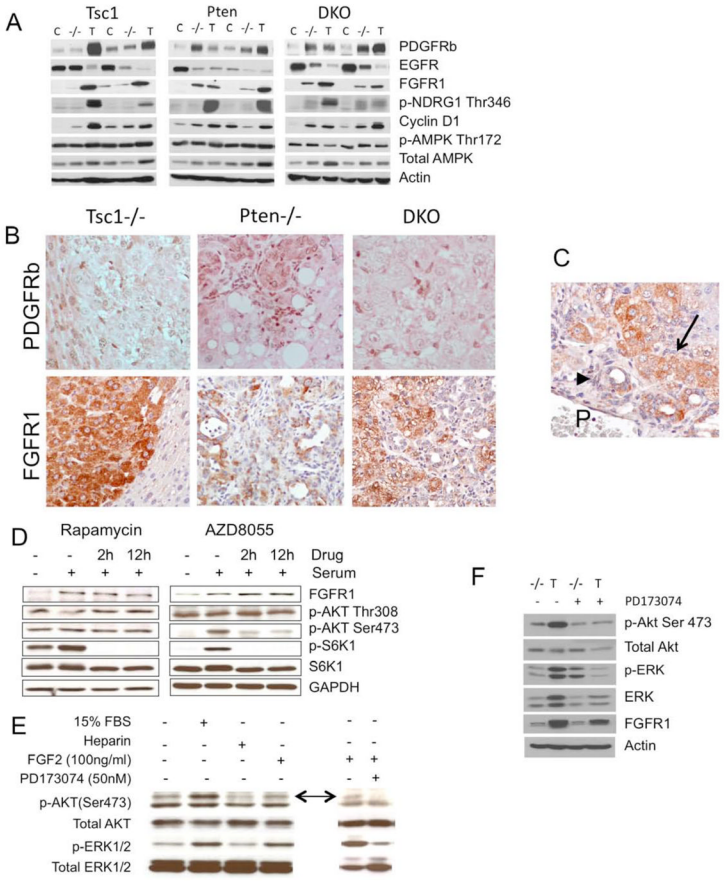

Figure 6.

Receptor tyrosine kinase expression in experimental liver tumors. A) Immunoblot analyses of liver tumors (T), adjacent non-tumor livers (−/−) and Cre-negative control livers (C) from the three models using indicated antibodies. B) IHC analyses of PDGFRb and FGFR1 in each of the 3 models. Magnification: 200X. C) FGFR1 expression in an early, peri-portal mixed tumor. P, portal vein. Arrowhead: ICC. Arrow: HCC. D) Immunoblot analyses showing FGFR1 expression and Akt/mTORC1 signaling in human hepatoma cells, HepG2, treated with rapamycin (100nM) (left column) and rat hepatoma cells (McA-RH7777) treated with AZD8055 (80nM) (right column). E) Activation of Akt and MAPK by FGF2 in hepatoma cells is suppressed by PD173074, a selective FGFR1 inhibitor. Arrows indicate p-Akt(Ser473). F) Inhibition of *Tsc1*−/− tumor (T) Akt and MAPK activities by PD173074 (20 mg/kg ip, daily for four days) compared to vehicle control-treated mice. −/− indicates non-tumor livers.

Table 1

Frequency of tumor subtypes in transgenic mice harboring liver tumors.

Genotype	HCC	ICC	HCC-ICC
Pten−/− (n=9)*	22%	90%	11%
Tsc1−/− (n=21)	100%	19%	0%
DKO (n=19)	79%	95%	58%

* number of mice per group. Each liver may contain multiple tumor types.